PHYSICAL SCIENCE

10.1126/sciadv.1601186

X-ray laser–induced electron dynamics observed by femtosecond diffraction from nanocrystals of Buckminsterfullerene

Brian Abbey,[1] Ruben A. Dilanian,[2]* Connie Darmanin,[1] Rebecca A. Ryan,[2] Corey T. Putkunz,[2] Andrew V. Martin,[2] David Wood,[3] Victor Streltsov,[4] Michael W. M. Jones,[5] Naylyn Gaffney,[6] Felix Hofmann,[7] Garth J. Williams,[8] Sébastien Boutet,[9] Marc Messerschmidt,[10] M. Marvin Seibert,[11] Sophie Williams,[2] Evan Curwood,[12] Eugeniu Balaur,[1] Andrew G. Peele,[5] Keith A. Nugent,[1] Harry M. Quiney[2]*

X-ray free-electron lasers (XFELs) deliver x-ray pulses with a coherent flux that is approximately eight orders of magnitude greater than that available from a modern third-generation synchrotron source. The power density of an XFEL pulse may be so high that it can modify the electronic properties of a sample on a femtosecond time scale. Exploration of the interaction of intense coherent x-ray pulses and matter is both of intrinsic scientific interest and of critical importance to the interpretation of experiments that probe the structures of materials using high-brightness femtosecond XFEL pulses. We report observations of the diffraction of extremely intense 32-fs nanofocused x-ray pulses by a powder sample of crystalline C_{60}. We find that the diffraction pattern at the highest available incident power significantly differs from the one obtained using either third-generation synchrotron sources or XFEL sources operating at low output power and does not correspond to the diffraction pattern expected from any known phase of crystalline C_{60}. We interpret these data as evidence of a long-range, coherent dynamic electronic distortion that is driven by the interaction of the periodic array of C_{60} molecular targets with intense x-ray pulses of femtosecond duration.

INTRODUCTION

To investigate the mechanisms of electronic damage during femtosecond x-ray diffraction measurements from nanocrystals, we devised an experiment in which a powdered sample of crystalline C_{60} was subjected to XFEL pulses of varying intensity (*1*–*6*). When subjected to intense XFEL pulses, graphite and amorphous carbon have recently been shown to exhibit some highly unusual properties (*7*, *8*). Here, we demonstrate that during interaction with a highly focused, high-energy pulse of x-rays, crystalline C_{60} undergoes a marked transition to an electronic state of lower symmetry. The experiment in which this effect was observed used a 10-keV (1.24 Å wavelength) x-ray beam, which was produced at the Linac Coherent Light Source (LCLS) (*1*) and focused by a Kirkpatrick-Baez (KB) mirror system to an area of less than 300-nm^2 full width at half maximum (FWHM) with a per-pulse fluence of 7.5×10^{11} photons at peak power. The number of photons per pulse was estimated using the pulse energy (in mJ), and images of the beam were taken before and after the mirrors to account for reflectivity losses and beam clipping. The sample was a fixed target of C_{60} nanocrystals, each of which was comparable in size to the beam, demonstrated by the fact that each XFEL shot produced a collection of Bragg spots from a small number of differently oriented crystals. The sample was produced by crushing 99.9+% pure, macroscopic C_{60} powder (*9*). A layer, thin enough to be within the ~100-μm depth of focus, produced by the KB system was supported by a 10-μm-thick kapton polyimide backing. At this energy, the scattered kapton background (which primarily occurs at low scattering angles) can readily be subtracted from the C_{60} data. The sample was continuously scanned in the beam at a pulse repetition rate of 1 Hz with a pulse length of ~32-fs FWHM. The x-ray pulse duration cannot be measured directly but can be estimated from the electron bunch length, which is determined by dispersing the electrons using a rapidly oscillating field. The x-ray pulse is typically around 60% of the electron pulse length. This value was used to estimate the x-ray pulse length from the measured electron pulse length. Attenuation upstream of the sample (Fig. 1) allowed the incident intensity to vary between 10 and 100% of the maximum value, permitting the introduction of intensity variations without changing samples or disrupting the vacuum conditions.

RESULTS

Forward-scattered diffraction data (Fig. 2, A to C) were collected at an estimated peak power density of 8.5×10^{19} W cm^{-2} when unattenuated, using the Cornell-SLAC pixel array detector (CSPAD) (*6*) containing 1516×1516 square pixels, each with an area of 110 μm^2, placed 79-mm downstream of the sample plane. Figure 2B shows an enlargement of data collected using a beam attenuated to 10% of the incident peak power, and Fig. 2C shows an enlargement of the same region with the attenuator removed. The pulse energy from the LCLS undergoes significant

[1]Australian Research Council (ARC) Centre of Excellence in Advanced Molecular Imaging, Department of Chemistry and Physics, La Trobe Institute for Molecular Sciences, La Trobe University, Bundoora, Victoria 3086, Australia. [2]ARC Centre of Excellence in Advanced Molecular Imaging, School of Physics, University of Melbourne, Parkville, Victoria 3010, Australia. [3]Department of Physics, Imperial College London, London SW7 2AZ, UK. [4]Florey Institute of Neuroscience and Mental Health, 30 Royal Parade, Parkville, Victoria, 3052, Australia. [5]Australian Synchrotron, 800 Blackburn Road, Clayton, Victoria 3168, Australia. [6]Swinburne University of Technology, Melbourne, Victoria 3122, Australia. [7]Department of Engineering Science, University of Oxford, Parks Road, Oxford OX1 3PJ, UK. [8]Brookhaven National Laboratory, PO Box 5000, Upton, NY 11973–5000, USA. [9]Linac Coherent Light Source, SLAC National Accelerator Laboratory, 2575 Sand Hill Road, Menlo Park, CA 94025, USA. [10]BioXFEL Science and Technology Center, 700 Ellicott Street, Buffalo, NY 1420, USA. [11]Laboratory of Molecular Biophysics, Department of Cell and Molecular Biology, Uppsala University, Husargatan 3 (Box 596), SE-751 24 Uppsala, Sweden. [12]Florey Institute of Neuroscience and Mental Health, Heidelberg, Victoria 3084, Australia.
*Corresponding author. Email: quiney@unimelb.edu.au (H.M.Q.); rubend@unimelb.edu.au (R.A.D.)

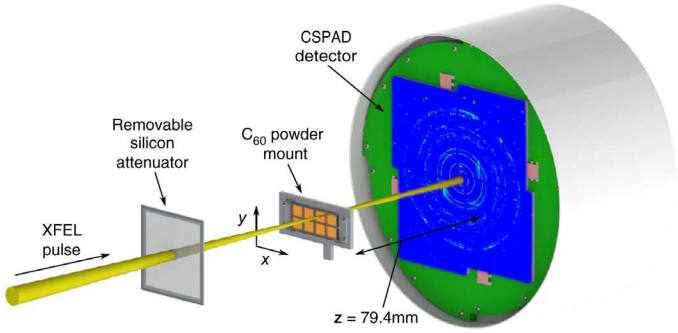

Fig. 1. Schematic of the experimental geometry used to collect the diffraction data. XFEL pulses (10 keV, 32 fs) acted as a simultaneous pump and probe when passing through the C_{60} nanocrystal powder sample, which was supported on a thin kapton film. A removable silicon attenuator upstream of the sample controlled the incident intensity and could be inserted for 10% or removed for 100% incident beam power. An aluminum attenuator (not shown) was placed directly in front of the CSPAD detector downstream of the sample to prevent the pixels from saturating. The direct beam passed through a small aperture in the CSPAD detector modules.

shot-to-shot variation, where data from each attenuator setting were selected so that only the highest incident power pulses (more than 50% of the mean pulse energy) were retained. The direct beam was allowed to pass through a gap in the center of the CSPAD detector modules. Bragg diffraction data of more than 1000 single-shot measurements were summed to produce a powder pattern for both the attenuated (referred to here as "10% XFEL data") and the unattenuated ("100% XFEL data") diffraction data (Fig. 2D) with a C_{60} powder outer ring resolution of around 2 Å. Synchrotron microdiffraction data were also collected at the MX2 beamline at the Australian Synchrotron (AS) using the same sample of C_{60}. An incident x-ray energy of 12.905 keV (λ = 0.9607 Å) was used. Structural analysis of the data showed that the measured diffraction patterns are indistinguishable from the room temperature face-centered cubic (FCC) phase of C_{60} with the unit cell parameter a = 14.20(3) Å (*10*).

A significant dependence of the diffraction pattern on incident intensity is observed for diffraction angles for which $2\theta \geq 20°$, whereas the diffraction pattern collected at lower resolution is comparatively insensitive to the incident intensity. Structural analysis shows that the 10% XFEL data and the AS powder diffraction patterns correspond to the standard room temperature FCC structure of C_{60} (*13*), twinned along the [111] direction of the crystal lattice. The twinned FCC structure is defined by the stacking sequence of close-packed (111) planes; the presence of such stacking faults leads to the displacement of Bragg reflections from their ideal positions (*11*). The directions of such displacements are dependent on the identity of the reflection.

The room temperature diffraction pattern of crystalline C_{60} indicates that there is no preferred orientation of the molecules in the FCC lattice because of rapid molecular rotation. The 10% XFEL data and the data collected at the AS are essentially identical and satisfy the selection rules on forbidden reflections in twinned FCC structures composed of centrosymmetric molecules (see Materials and Methods). However, the data collected at 100% peak power using XFEL pulses violate these selection rules and do not correspond to the low-temperature structure of C_{60}, which involves orientational alignment of molecules in the lattice (*12*).

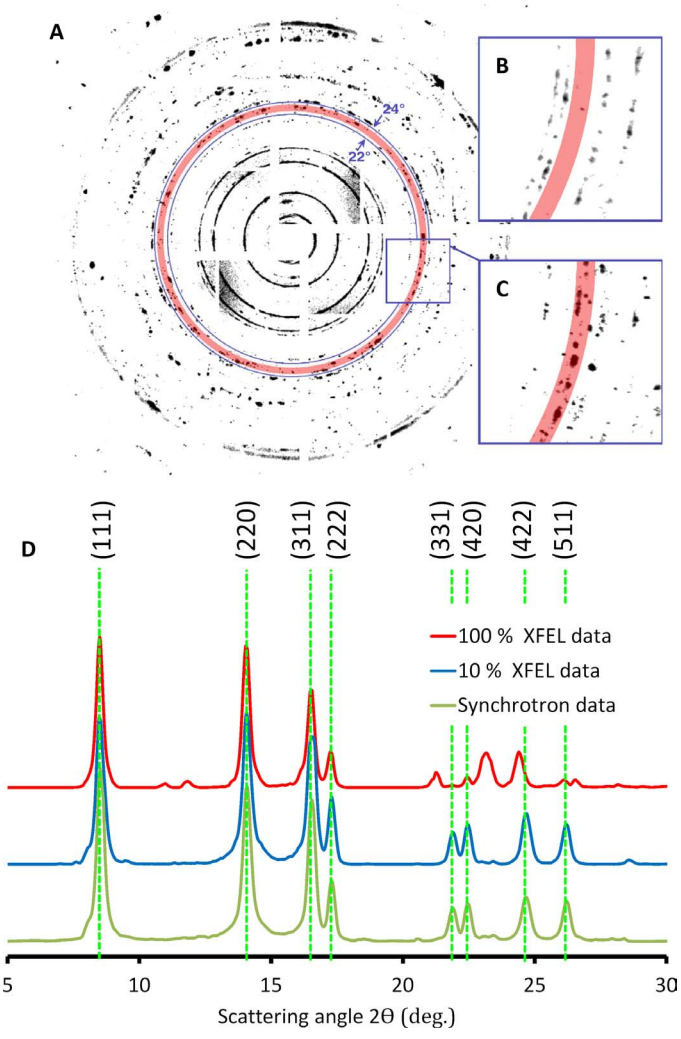

Fig. 2. C_{60} diffraction data. (**A**) Summed diffraction data from 2500 single shots recorded at 100% power. The semitransparent red circle indicates the location of one of the reflections only observed in the 100% XFEL data. (**B**) Enlarged region from (A) showing Bragg peaks at 10% power, consistent with the room temperature FCC structure. (**C**) The same region as in (B) collected at 100% power. To enhance contrast, $\sqrt{I}$ has been displayed. (**D**) Azimuthally averaged experimental XFEL data for 10 and 100% incident power and synchrotron data collected from the same C_{60} sample. Vertical lines indicate positions of FCC Bragg reflections. Between 20° and 28°, significant differences are observed between the synchrotron and the 10 and 100% XFEL data.

DISCUSSION

The marked dependence of the Bragg diffraction pattern on the incident XFEL pulse intensity cannot be explained within the framework of the standard FCC structure. Comparison of the powder patterns for the 10 and 100% XFEL data (Fig. 2, E and F, respectively) shows a clear suppression of the intensity of some peaks and a marked increase in others for the 100% XFEL data at a resolution higher than 3.5 Å ($2\theta \geq 20°$). These observations provide direct evidence that the scattering factors of the C_{60} molecules are modified by the XFEL pulse in a manner that preserves the translational symmetry of the twinned C_{60} crystal. The data suggest that a new, albeit transient, crystalline phase of C_{60} has

been created through interaction with the nanofocused XFEL beam. Our results indicate that there is a critical incident intensity that precipitates the onset of this coherent electronic rearrangement in C_{60}. From our data, we can conclude that this point lies somewhere between 10 and 100% of the incident intensity used in this experiment. The goal of future experiments conducted on this system will be to more precisely determine this threshold intensity.

The experimental conditions under which the transient state forms at the XFEL permit us to distinguish our observation from other, optically driven, ultrafast electronic phenomena in C_{60}. Decoupling of the electron density from the underlying nuclear structure (*13*, *14*) has previously been observed using ultraviolet spectroscopy. Other low-energy, short-range, collective electronic effects, such as giant dipole plasmon resonance, are well established in single-molecule studies (*15*) and small-cluster samples of C_{60} (*16*). However, transient, long-range, coherent modifications to the electronic structure of C_{60} crystals appear to have been neither reported nor predicted previously.

To explain the observed diffraction of C_{60} at 100% peak power, we seek to identify an electronic process involving a coherent redistribution of electron density on a femtosecond time scale. This is in contrast to a classical change in structural phase involving either the lattice parameters or the individual C_{60} molecules, which is presumed to occur on a much longer time scale. The probability of direct ionization of the outer shells in comparison to the core shells is negligible for a femtosecond XFEL pulse; inner-shell photoionization must initiate the electronic processes that follow. If we assume that inner-shell photoionization is a stochastic process and that the inner-shell vacancies remain localized to atomic centers, this process on its own would simply introduce disorder into the system and a diffuse background to the observed diffraction data. Therefore, secondary electronic events seem most likely to be driving the observed dynamical change in the electron distribution, which is the physical quantity that is probed in a diffraction experiment using a femtosecond XFEL pulse. Auger decay fills the inner-shell vacancies, ejecting a low-energy electron and creating a valence shell hole. In neutral species involving first-row elements, this process occurs on a time scale of 5 to 10 fs but is generally faster in highly ionized molecular species. Whereas inner-shell holes are regarded as localized to atomic sites, valence shell holes in ionized C_{60} are likely to be highly mobile because they are allocated to partially occupied delocalized molecular orbitals. The rapid inner-shell photoionization of the C_{60} molecules generates a strong internal electric field in the crystal, whereas the valence shells continue to be ionized by ejected photoelectrons and Auger electrons. Combined with the high mobility of holes in the valence shells of ionized C_{60} and the short duration of the interaction with the XFEL pulse, these factors all indicate that the observed effect should be attributed to a rapid and coherent redistribution of the electron distribution. After a few tens of femtoseconds have elapsed, a large number of electrons will leave the system with a large kinetic energy. This leaves the system in a highly ionized state, which inevitably leads to melting of the lattice and the formation of a plasma, followed eventually by Coulomb explosion of the ionic fragments.

We constructed a forward model for the C_{60} crystalline diffraction pattern modified by interaction with the XFEL pulse at 100% peak intensity by including both twinning of the FCC lattice and collective alignment of ionized molecules. Adding the effect of the collective alignment of the non-centrosymmetric C_{60} molecule ions (depicted in Fig. 3A) to give a combined contribution from both effects provides a good match to the 100% XFEL data (Fig. 3B).

In conclusion, we have observed a new transient electronic phase of C_{60}, which exists during the interaction of the widely studied and well-characterized fullerene C_{60} with a highly focused, 32-fs XFEL pulse. Surprisingly, the ionization of a significant fraction of the atoms in the C_{60} crystals does not, as one might expect, lead to disorder. We suggest here that it induces a different kind of ordering of the electronic structure, resulting in a significant rearrangement of Bragg peaks in the crystalline diffraction pattern. This results not in a subtle change in the diffraction data but rather in a wholesale modification that is the characteristic signature of long-range rearrangement of the electronic structure. Our interpretation of the results suggests that the effects reported here require a high degree of molecular symmetry and electron-hole mobility in the ionized state; however, it is by no means certain that similar femtosecond electronic rearrangement will be absent from structures consisting of lower-symmetry molecules. These are open questions that can only be answered through further experiments. What is clear is that the discovery of a new (transient) crystal structure for Buckminsterfullerene suggests that there exists a new class of long-range, coherent electron dynamics in crystals that can now be explored using x-ray lasers.

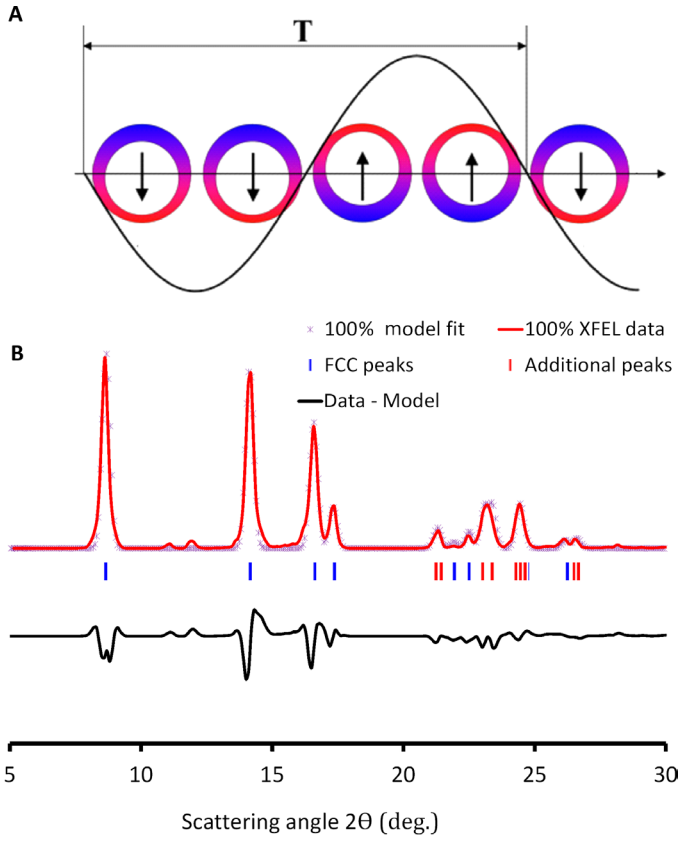

Fig. 3. Comparing experimental and simulated data. (**A**) Schematic representation of the alignment of polarized C_{60} molecules. (**B**) Comparison of the 100% XFEL data and the model prediction based on the newly predicted, lower symmetry, structure. Directly below the plot are tick marks indicating the predicted model peak positions; because of the finite experimental resolution, not all of these peaks are resolved in the data. The black line shows the difference between the model and experimental data.

MATERIALS AND METHODS

We were able to accurately fit the XFEL data at 100% incident power using a modified, periodically varying molecular form factor (MFF). To construct a crystallographic model that matches the 100% XFEL data, we postulated a simple asymmetric molecular charge distribution in which the spherical electron distribution of the mth molecule is displaced relative to its position in the room temperature crystal structure by an amount of δr_m. Interaction with the XFEL pulse resulted in the ionization of the C_{60} molecules throughout the scattering volume. The resulting electric field associated with the remaining positive C_{60} ions located at FCC lattice positions induced polarization of the molecular electron density, which produced an array of electric dipoles. We assumed that this periodic distribution of electric dipoles can evolve into a stable and ordered configuration on a femtosecond time scale. Because the diffraction pattern suggests that the charge displacement has long-range periodicity, the displacements of the charge distribution will have the functional form

$$\delta r_m = \delta r \sin(2\pi \vec{r}_m \cdot \vec{T}) \quad (1)$$

where $\vec{r}_m = n_{1m}\vec{a} + n_{2m}\vec{b} + n_{3m}\vec{c}$ defines the lattice vector of molecule m with lattice parameters a, b, and c and where n_{1m}, n_{2m}, and n_{3m} are integers. $\vec{T}$ is a vector that describes both the direction and assumed periodicity of the charge displacement. Within this model, we found that a periodicity of the form ↑↑ ↓↓ ↑↑ (Fig. 3A) uniquely generates a diffraction pattern that matches the experimental data.

The corresponding intensity, $I(\vec{S})$, is then given by

$$I(\vec{S}) = KL_p \left| \Phi(\vec{S}) \sum_{m=1}^{M} \exp\left(-2\pi i \vec{S} \cdot (\vec{r}_m + \delta \vec{r}_m)\right) \right|^2 w(\vec{S}) \quad (2)$$

where $\vec{S}$ is the scattering vector, K is an experimental scaling factor, L_p is the Lorentz polarization factor, $w(\vec{S})$ is the peak profile function, and M is the total number of C_{60} molecules contained within the scattering volume. $\Phi(\vec{S})$ is the MFF, whereas $\delta \vec{r}_m$ describes the displacement of charge from its neutral position whose direction is given by

$$\delta \vec{r}_m = \delta r_m \frac{\vec{T}}{|\vec{T}|} \quad (3)$$

We note that in the limit $|\delta \mathbf{r}_m| \to 0$, Eq. 2 reduces to the intensity formula used to calculate the room temperature C_{60} diffraction pattern.

This structural interpretation of the C_{60} XFEL data requires neither a change in lattice parameters or symmetry of the lattice nor the relocation of the atomic positions. Figure 3B shows that this model accurately describes the significant reduction of intensities of the reflections associated with the FCC lattice observed in the 100% powder diffraction data, as well as the appearance of additional reflections over the range of data collected. All peaks predicted by this model were observed in the experiment. Below 5°, the x-rays passed through the central aperture of the detector, whereas above 30°, no more diffracted intensity from C_{60} was measured above background.

In our model, we required a sufficient level of ionization to match the experimental data. The process was initiated by the interaction of the femtosecond XFEL pulse with the crystalline C_{60}, which is dominated (by around two orders of magnitude) by inner-shell (1*s* orbital) photoionization. In the 100% intensity case, we estimated that, assuming a 300×300–nm focal spot size and 10^{12} photons per pulse, every molecule in the crystal is ionized at least once within a few femtoseconds. This estimate suggests that the level of inner-shell photoionization required by our model can occur on a time scale much shorter than the Auger lifetime of 10 fs.

REFERENCES AND NOTES

1. P. Emma, R. Akre, J. Arthur, R. Bionta, C. Bostedt, J. Bozek, A. Brachmann, P. Bucksbaum, R. Coffee, F.-J. Decker, Y. Ding, D. Dowell, S. Edstrom, A. Fisher, J. Frisch, S. Gilevich, J. Hastings, G. Hays, Ph. Hering, Z. Huang, R. Iverson, H. Loos, M. Messerschmidt, A. Miahnahri, S. Moeller, H.-D. Nuhn, G. Pile, D. Ratner, J. Rzepiela, D. Schultz, T. Smith, P. Stefan, H. Tompkins, J. Turner, J. Welch, W. White, J. Wu, G. Yocky, J. Galayda, First lasing and operation of an ångstrom-wavelength free-electron laser. *Nat. Photonics* **4**, 641–647 (2010).
2. L. Young, E. P. Kanter, B. Krässig, Y. Li, A. M. March, S. T. Pratt, R. Santra, S. H. Southworth, N. Rohringer, L. F. DiMauro, G. Doumy, C. A. Roedig, N. Berrah, L. Fang, M. Hoener, P. H. Bucksbaum, J. P. Cryan, S. Ghimire, J. M. Glownia, D. A. Reis, J. D. Bozek, C. Bostedt, M. Messerschmidt, Femtosecond electronic response of atoms to ultra-intense X-rays. *Nature* **466**, 56–61 (2010).
3. K. Nass, L. Foucar, T. R. M. Barends, E. Hartmann, S. Botha, R. L. Shoeman, R. B. Doak, R. Alonso-Mori, A. Aquila, S. Bajt, A. Barty, R. Bean, K. R. Beyerlein, M. Bublitz, N. Drachmann, J. Gregersen, H. O. Jönsson, W. Kabsch, S. Kassemeyer, J. E. Koglin, M. Krumrey, D. Mattle, M. Messerschmidt, P. Nissen, L. Reinhard, O. Sitsel, D. Sokaras, G. J. Williams, S. Hau-Riege, N. Timneanu, C. Caleman, H. N. Chapman, S. Boutet, I. Schlichting, Indications of radiation damage in ferredoxin microcrystals using high-intensity X-FEL beams. *J. Synchrotron Radiat.* **22**, 225–238 (2015).
4. S. Boutet, L. Lomb, G. J. Williams, T. R. M. Barends, A. Aquila, R. B. Doak, U. Weierstall, D. P. DePonte, J. Steinbrener, R. L. Shoeman, M. Messerschmidt, A. Barty, T. A. White, S. Kassemeyer, R. A. Kirian, M. M. Seibert, P. A. Montanez, C. Kenney, R. Herbst, P. Hart, J. Pines, G. Haller, S. M. Gruner, H. T. Philipp, M. W. Tate, M. Hromalik, L. J. Koerner, N. van Bakel, J. Morse, W. Ghonsalves, D. Arnlund, M. J. Bogan, C. Caleman, R. Fromme, C. Y. Hampton, M. S. Hunter, L. C. Johansson, G. Katona, C. Kupitz, M. Liang, A. V. Martin, K. Nass, L. Redecke, F. Stellato, N. Timneanu, D. Wang, N. A. Zatsepin, D. Schafer, J. Defever, R. Neutze, P. Fromme, J. C. H. Spence, H. N. Chapman, I. Schlichting, High-resolution protein structure determination by serial femtosecond crystallography. *Science* **337**, 362–364 (2012).
5. H. N. Chapman, P. Fromme, A. Barty, T. A. White, R. A. Kirian, A. Aquila, M. S. Hunter, J. Schulz, D. P. DePonte, U. Weierstall, R. B. Doak, F. R. N. C. Maia, A. V. Martin, I. Schlichting, L. Lomb, N. Coppola, R. L. Shoeman, S. W. Epp, R. Hartmann, D. Rolles, A. Rudenko, L. Foucar, N. Kimmel, G. Weidenspointner, P. Holl, M. Liang, M. Barthelmess, C. Caleman, S. Boutet, M. J. Bogan, J. Krzywinski, C. Bostedt, S. Bajt, L. Gumprecht, B. Rudek, B. Erk, C. Schmidt, A. Hömke, C. Reich, D. Pietschner, L. Strüder, G. Hauser, H. Gorke, J. Ullrich, S. Herrmann, G. Schaller, F. Schopper, H. Soltau, K.-U. Kühnel, M. Messerschmidt, J. D. Bozek, S. P. Hau-Riege, M. Frank, C. Y. Hampton, R. G. Sierra, D. Starodub, G. J. Williams, J. Hajdu, N. Timneanu, M. M. Seibert, J. Andreasson, A. Rocker, O. Jönsson, M. Svenda, S. Stern, K. Nass, R. Andritschke, C.-D. Schröter, F. Krasniqi, M. Bott, K. E. Schmidt, X. Wang, I. Grotjohann, J. M. Holton, T. R. M. Barends, R. Neutze, S. Marchesini, R. Fromme, S. Schorb, D. Rupp, M. Adolph, T. Gorkhover, I. Andersson, H. Hirsemann, G. Potdevin, H. Graafsma, B. Nilsson, J. C. H. Spence, Femtosecond X-ray protein nanocrystallography. *Nature* **470**, 73–77 (2011).
6. R. Neutze, R. Wouts, D. van der Spoel, E. Weckert, J. Hajdu, Potential for biomolecular imaging with femtosecond X-ray pulses. *Nature* **406**, 752–757 (2000).
7. J. Gaudin, O. Peyrusse, J. Chalupský, M. Toufarová, L. Vyšín, V. Hájková, R. Sobierajski, T. Burian, Sh. Dastjani-Farahani, A. Graf, M. Amati, L. Gregoratti, S. P. Hau-Riege, G. Hoffmann, L. Juha, J. Krzywinski, R. A. London, S. Moeller, H. Sinn, S. Schorb, M. Störmer, Th. Tschentscher, V. Vorlíček, H. Vu, J. Bozek, C. Bostedt, Amorphous to crystalline phase transition in carbon induced by intense femtosecond x-ray free-electron laser pulses. *Phys. Rev. B* **86**, 024103 (2012).
8. S. P. Hau-Riege, A. Graf, T. Döppner, R. A. London, J. Krzywinski, C. Fortmann, S. H. Glenzer, M. Frank, K. Sokolowski-Tinten, M. Messerschmidt, C. Bostedt, S. Schorb, J. A. Bradley, A. Lutman, D. Rolles, A. Rudenko, B. Rudek, Ultrafast transitions from solid to liquid and plasma states of graphite induced by x-ray free-electron laser pulses. *Phys. Rev. Lett.* **108**, 217402 (2012).
9. SES Research, Suite 106, Houston, TX 77092, USA.
10. H. W. Kroto, J. R. Heath, S. C. O'Brien, R. F. Curl, R. E. Smalley, C_{60}: Buckminsterfullerene. *Nature* **318**, 162–163 (1985).

11. M. S. Paterson, X-ray diffraction by face-centered cubic crystals with deformation faults. *J. Appl. Phys.* **23**, 805–811 (1952).
12. W. I. F. David, R. M. Ibberson, J. C. Matthewman, K. Prassides, T. J. S. Dennis, J. P. Hare, H. W. Kroto, R. Taylor, D. R. M. Walto, Crystal structure and bonding of ordered C_{60}. *Nature* **353**, 147–149 (1991).
13. S. Hellmann, M. Beye, C. Sohrt, T. Rohwer, F. Sorgenfrei, H. Redlin, M. Kalläne, M. Marczynski-Bühlow, F. Hennies, M. Bauer, A. Föhlisch, L. Kipp, W. Wurth, K. Rossnagel, Ultrafast melting of a charge-density wave in the Mott insulator 1*T*–TaS_2. *Phys. Rev. Lett.* **105**, 187401 (2010).
14. J. C. Petersen, S. Kaiser, N. Dean, A. Simoncig, H. Y. Liu, A. L. Cavalieri, C. Cacho, I. C. E. Turcu, E. Springate, F. Frassetto, L. Poletto, S. S. Dhesi, H. Berger, A. Cavalleri, Clocking the melting transition of charge and lattice order in 1*T*–TaS_2 with ultrafast extreme-ultraviolet angle-resolved photoemission spectroscopy. *Phys. Rev. Lett.* **107**, 177402 (2011).
15. I. V. Hertel, H. Steger, J. de Vries, B. Weisser, C. Menzel, B. Kamke, W. Kamke, Giant plasmon excitation in free C_{60} and C_{70} molecules studied by photoionization. *Phys. Rev. Lett.* **68**, 784–787 (1992).
16. G. Wendin, B. Wästberg, Many-electron effects in BaC_{60}: Collective response and molecular effects in optical conductivity and photoionization. *Phys. Rev. B* **48**, 14764–14767 (1993).

Acknowledgments

Funding: The authors acknowledge the support of the Australian Research Council Centre of Excellence in Advanced Molecular Imaging. Portions of this research were carried out at the LCLS, a national user facility operated by the Stanford University on behalf of the U.S. Department of Energy, Office of Basic Energy Sciences. We acknowledge the travel funding provided by the International Synchrotron Access Program managed by the AS and by the Australian government. In addition, some of this research was undertaken on the MX1 and MX2 beamlines at the AS, Victoria, Australia. **Author contributions:** B.A. was responsible for planning and managing all experimental aspects of the project. Experiments were designed by B.A., R.A.D., V.S., C.D., and G.J.W. B.A., H.M.Q., K.A.N., and R.A.D. wrote the original LCLS proposal. D.W., R.A.D., R.A.R., A.V.M., E.C., and S.W. carried out the simulation work. B.A., R.A.D., C.D., V.S., M.W.M.J., R.A.R., N.G., F.H., G.J.W., S.B., M.M., M.M.S., A.G.P., C.T.P., A.V.M., and K.A.N. collected the experimental data. C.T.P. and A.V.M. led the experimental data conversion and analysis. B.A., C.D., N.G., and E.B. were responsible for the sample holder design and testing. All authors contributed to the writing of the manuscript. The formulation of electronic damage within coherence theory is performed by H.M.Q. and K.A.N.; R.A.D. conceived the idea to apply this formalism to C_{60}. **Competing interests:** The authors declare that they have no competing interests. **Data and materials availability:** All data needed to evaluate the conclusions in the paper are present in the paper. Additional data related to this paper may be requested from the authors.

Submitted 26 May 2016
Accepted 9 August 2016
Published 9 September 2016
10.1126/sciadv.1601186

Citation: B. Abbey, R. A. Dilanian, C. Darmanin, R. A. Ryan, C. T. Putkunz, A. V. Martin, D. Wood, V. Streltsov, M. W. M. Jones, N. Gaffney, F. Hofmann, G. J. Williams, S. Boutet, M. Messerschmidt, M. M. Seibert, S. Williams, E. Curwood, E. Balaur, A. G. Peele, K. A. Nugent, H. M. Quiney, X-ray laser–induced electron dynamics observed by femtosecond diffraction from nanocrystals of Buckminsterfullerene. *Sci. Adv.* **2**, e1601186 (2016).

X-ray laser–induced electron dynamics observed by femtosecond diffraction from nanocrystals of Buckminsterfullerene

Brian Abbey, Ruben A. Dilanian, Connie Darmanin, Rebecca A. Ryan, Corey T. Putkunz, Andrew V. Martin, David Wood, Victor Streltsov, Michael W. M. Jones, Naylyn Gaffney, Felix Hofmann, Garth J. Williams, Sébastien Boutet, Marc Messerschmidt, M. Marvin Seibert, Sophie Williams, Evan Curwood, Eugeniu Balaur, Andrew G. Peele, Keith A. Nugent and Harry M. Quiney

Sci Adv **2** (9), e1601186.
DOI: 10.1126/sciadv.1601186